Subaxolemmal Cytoskeleton in Squid Giant Axon. II. Morphological Identification of Microtubule- and Microfilament-associated Domains of Axolemma

Shoichiro Tsukita,* Sachiko Tsukita,* Takaaki Kobayashi,‡ and Gen Matsumoto§

*Department of Anatomy, Faculty of Medicine, University of Tokyo, Bunkyo-ku, Tokyo 113; ‡Department of Biochemistry, Jikei University, School of Medicine, Minato-ku, Tokyo 105; §Electrotechnical Laboratory, Tsukuba Science City, Ibaraki 305, Japan. The present address of Drs. Shoichiro Tsukita and Sachiko Tsukita is Ultrastructural Research Section, Tokyo Metropolitan Institute of Medical Science, Honkomagome, Bunkyo-ku, Tokyo 113, Japan.

Abstract. In the preceding paper (Kobayashi, T., S. Tsukita, S. Tsukita, Y. Yamamoto, and G. Matsumoto, 1986, *J. Cell Biol.*, 102:1710–1725), we demonstrated biochemically that the subaxolemmal cytoskeleton of the squid giant axon was highly specialized and mainly composed of tubulin, actin, axolinin, and a 255-kD protein. In this paper, we analyzed morphologically the molecular organization of the subaxolemmal cytoskeleton in situ. For thin section electron microscopy, the subaxolemmal cytoskeleton was chemically fixed by the intraaxonal perfusion of the fixative containing tannic acid. With this fixation method, the ultrastructural integrity was well preserved. For freeze-etch replica electron microscopy, the intraaxonally perfused axon was opened and rapidly frozen by touching its inner surface against a cooled copper block (4°K), thus permitting the direct stereoscopic observation of the cytoplasmic surface of the axolemma. Using these techniques, it became clear that the major constituents of the subaxolemmal cytoskeleton were microfilaments and microtubules. The microfilaments were observed to be associated with the axolemma through a specialized meshwork of thin strands, forming spot-like clusters just beneath the axolemma. These filaments were decorated with heavy meromyosin showing a characteristic arrowhead appearance. The microtubules were seen to run parallel to the axolemma and embedded in the fine three-dimensional meshwork of thin strands. In vitro observations of the aggregates of axolinin and immunoelectron microscopic analysis showed that this fine meshwork around microtubules mainly consisted of axolinin. Some microtubules grazed along the axolemma and associated laterally with it through slender strands. Therefore, we were led to conclude that the axolemma of the squid giant axon was specialized into two domains (microtubule- and microfilament-associated domains) by its underlying cytoskeletons.

At the node of Ranvier of mammalian myelinated axons, the close association between the excitable axolemma and the underlying cytoskeletal structures has often been pointed out (27), and the physiological role of this association has been a subject of hot debate (4, 12). For correlative biochemical and morphological studies of the interaction between the excitable axolemma and the axonal cytoskeleton, the squid giant axon serves as a model system. In the preceding paper (15), we analyzed biochemically the molecular organization of the subaxolemmal cytoskeleton of squid giant axons and showed that the subaxolemmal axoplasm was highly specialized. The subaxolemmal cytoskeleton was mainly composed of tubulin, actin, and their associated unique high-molecular-weight proteins (axolinin and the 255-kD protein). To understand how these proteins are organized into the cytoskeletal network in situ, detailed morphological analyses of the subaxolemmal cytoskeleton are required. Using scanning electron microscopy, Metuzals and Tasaki (22) have successfully visualized the well-developed cytoskeletal network underlying the axolemma of squid giant axon and shown that this network may contain actin-like filaments. On the other hand, Endo et al. (5) and Hodge and Adelman (10) have observed that this subaxolemmal cytoskeleton is mainly composed of longitudinally oriented microtubules under thin section electron microscopy. This discrepancy may be due to the difficulty of preserving the ultrastructural integrity of the subaxolemmal cytoskeleton by the conventional chemical fixation. Therefore, the detailed morphological analysis of the molecular organization of the subaxolemmal cytoskeleton in squid giant axon appears to require some new preparation methods.

One of the advantages of using squid giant axons is that various kinds of solutions can be intraaxonally perfused. Thus, we tried to chemically fix the subaxolemmal cytoskeleton by the intraaxonal perfusion of the fixatives containing tannic acid, and it became clear that with this fixation method

the preservation of its fine structural integrity was very much improved. Furthermore, we developed a new preparation method for freeze-etch replica electron microscopy which permitted the stereoscopic observation of the association of the cytoskeletons with the cytoplasmic surface of the axolemma of squid giant axons. In this paper, with these new preparation methods combining the heavy meromyosin (HMM)[1] decoration and antibody decoration technique, we analyzed the molecular organization of the subaxolemmal cytoskeleton in situ of the squid giant axons and obtained evidence that the axolemma can be divided into two domains, one microtubule associated and the other microfilament associated. We believe this study provides us with the first step in analyzing how sodium and potassium channels interact with subaxolemmal cytoskeletons in situ of squid giant axons.

Materials and Methods

All materials and methods used in this study are described in the preceding paper (15). Procedures applied specifically for observations to be reported in this paper are given below.

Intraaxonal Perfusion of Squid Giant Axon

The nerve of the squid, *Dorytheuthis bleekeri*, containing a giant axon was carefully dissected out with both ends tightly ligated using fine threads. The nerve was put on a transparent rubber, one end was cut off, and the axoplasm of the giant axon was gently squeezed out using a rubber-coated roller. The nerve was then transferred to a chamber filled with artificial sea water and intraaxonally perfused with the standard internal solution (SIS) containing 380 mM KF, 20 mM K-Hepes buffer (pH 7.25) and 4% glycerol under measurement of the excitability of the giant axon (1, 26).

Thin Section Electron Microscopy

The subaxolemmal cytoskeleton was chemically prefixed by changing the perfusion solution from SIS to the chemical fixative containing 2.5% glutaraldehyde, 2% formaldehyde, 0.5% tannic acid, 1 mM EGTA, and 0.1 M sodium cacodylate buffer (pH 7.4). The fixative was further perfused for 5 min after the excitability of the giant axon had completely disappeared. The nerve was then rinsed in the same fixative at room temperature for 30 min, and cut into small pieces. Fixation was continued for 3 h at 4°C, and then the samples were washed with 0.1 M sodium cacodylate buffer (pH 7.4) and postfixed with 1% OsO_4 in 0.1 M sodium cacodylate buffer (pH 7.4) for 2 h at 4°C. After being rinsed in distilled water, samples were stained en bloc with 0.5% aqueous uranyl acetate for 2 h at room temperature, dehydrated in graded concentrations of ethanol, and embedded in Epon 812. Thin sections were cut with a diamond knife, stained doubly with uranyl acetate and lead citrate, and examined in a Hitachi 11-DS electron microscope at an accelerating voltage of 75 kV.

Rapid-freeze, Deep-etch, Rotary-shadow Replica Electron Microscopy

After perfusion with SIS as described above, the giant axon was further intraaxonally perfused with a fixative composed of 2.5% glutaraldehyde, 1 mM EGTA, and 0.1 M sodium cacodylate buffer (pH 7.4). The perfusion was continued for 10 min and the nerve was then rinsed in the same fixative at room temperature for 30–60 min. After fixation, to expose the inner face of the giant axon in the perfusion zone, the giant axon was longitudinally cut into two pieces with a sharp razor blade under the dissecting microscope. The opened axon was then rinsed in the distilled water containing 10% methanol for 10 min and mounted with its inner face up on a specimen holder for rapid freezing. Some axons were opened in the SIS without chemical fixation and immediately mounted on a specimen holder.

The rapid-freeze, deep-etch replica method (8, 9) used in this study has been previously described in detail (36, 37, 39). The opened axon on a specimen holder was rapidly frozen by touching its inner face against a pure copper block cooled to 4°K by liquid helium using an Eiko freezing apparatus, RF-10 (Eiko Engineering, Mito, Japan). The frozen samples were stored in liquid nitrogen.

[1] *Abbreviations used in this paper:* HMM, heavy meromyosin; SIS, standard internal solution.

For deep-etching and replication, the frozen samples on the holder were transferred to a cryokit (FTC/LTS-2) fitted to a Sorval MT-2 ultramicrotome and cut with glass knives at −120°C to remove the outermost metal-contact surface of the sample. The preferable depth of removal was 10–20 μm. After cutting, the sample with a mirror-smooth face was transferred to liquid nitrogen in a small cup and put into an Eiko freeze-etch device, FD-3 (Eiko Engineering) together with the specimen holder using a carrier with a cooled cover. In the device, the exposed surface was deeply etched in vacuo (1×10^{-7} mmHg) at −95°C for 8–10 min followed by rotary-shadowing with platinum (30°) and carbon (90°). The sample was then removed from the freeze-etch device and immersed in bleach (almost 100% sodium hypochloride). The replicas floating off the sample were washed three times with distilled water and picked up on formvar-filmed grids. The replicas were examined in a JEOL 1200EX electron microscope equipped with a tilting stage at an accelerating voltage of 100 kV. Stereo pair electron micrographs were taken by tilting the specimen stage at ±10°. Electron microscope negatives were routinely contact reversed and then printed as negative images.

HMM Decoration (11)

After perfusion with SIS, some axons were intraaxonally perfused for 20 min with the SIS containing 3 mg/ml HMM obtained from rabbit skeletal muscle. The perfusion solution was then changed to SIS (20 min) and then to the fixative containing 2.5% glutaraldehyde, 2.0% formaldehyde, 1 mM EGTA, 0.5% tannic acid, and 0.1 M cacodylate buffer (pH 7.0). The nerve was then treated for thin section electron microscopy as described above.

Immunofluorescence Labeling

Antisera to the purified axolinin were elicited in rabbits as described in the preceding paper (15). For indirect immunofluorescence microscopy, the squid nerves containing a giant axon were rapidly removed and frozen in Freon 13 cooled with liquid nitrogen. The frozen sections (~10 μm thick) were cut in a cryostat, mounted on ovalbumin-treated glass slides, air dried, and fixed in methanol at −20°C for 10 min. After being washed twice in phosphate-buffered saline (PBS), the sections were pretreated with non-immune goat serum for 1 h. They were then washed in PBS and incubated with rabbit anti-axolinin antibody for 1 h at room temperature. After being washed three times in PBS, the rabbit anti-axolinin antibody was labeled by incubation of the sections with fluorescein isothiocyanate–conjugated goat anti-rabbit IgG. The sections were then washed three times in PBS and examined with an Olympus fluorescence microscope.

Immunoelectron Microscopic Labeling

After the central part of the axoplasm was extruded out, the giant axon was intraaxonally perfused with SIS for 15 min and then with the fixative for 5 min. The fixative was composed of 0.5% glutaraldehyde, 2 mM EGTA, and 100 mM Hepes buffer (pH 7.0). The nerve was then rinsed in the same fixative and the giant axon was longitudinally cut into two pieces to expose the subaxolemmal cytoskeleton. The fixation was continued for 10 min in total at room temperature and the opened axon was washed four times in solution-G (95 mM potassium glutamate, 10% glycerol, 5 mM phosphate buffer, pH 7.2). The following steps were all done at 20°C. The opened axon was then transversely cut into small pieces ~1 mm in length. Each piece was treated with sodium borohydride (1 mg/ml) in solution-G for 20 min; washed three times in solution-G + 0.1% bovine serum albumin (BSA); incubated in normal goat serum (diluted 1:20 in solution-G + 0.1% BSA) for 10 min; washed twice in solution-G + 0.1% BSA. The sample was subsequently incubated with the anti-axolinin antibody (diluted 1:10 in solution-G + 0.1% BSA) for 4 h. Control preparations were incubated for the same time in preimmune serum (diluted 1:10 in solution-G + 0.1% BSA). After incubation with the primary antibodies, the samples were washed four times in solution-G + 0.1% BSA for 15 min and incubated with the secondary antibody (goat anti-rabbit IgG) coupled to 10-nm gold (GAR-G10) (Janssen Life Science Products) for 12 h. GAR-G10 was diluted 1:2 in solution-G + 0.1% BSA. The axons were washed in solution-G + 1% BSA three times for 20 min, followed by fixation with 2.5% glutaraldehyde, 0.2% tannic acid, and 0.1 M phosphate buffer (pH 7.0) for 2 h. The samples were further processed for thin section electron microscopy as described above.

Low-angle Rotary-shadowing Electron Microscopy

The following preparations were examined by low-angle rotary-shadowing electron microscopy, mainly according to the method developed by Tyler and Branton (38): (*a*) axolinin (25 μg/ml) in 0.6 M NaCl, 50% glycerol, MES buffer

(pH 6.8) (solution-M); (*b*) axolinin (25 μg/ml) in 0.1 M KCl, 50% glycerol, and 10 mM MES buffer (pH 6.8); (*c*) axolinin (2.5 μg/ml) and tubulin (35 μg/ml) in solution-M; (*d*) tubulin (35 μg/ml) in solution-M. These preparations were sprayed onto freshly cleaved mica. The droplets on the mica were dried at room temperature under vacuum (1×10^{-6} Torr) in an Eiko freeze-etch device FD-2 (Eiko Engineering, Mito, Japan) for 10 min. Platinum was then rotary-shadowed at an angle of 5° followed by a coating from above with carbon. The replica was floated off on distilled water and picked up on formvar-filmed grids. The samples were examined in a Hitachi 11-DS electron microscope at an accelerating voltage of 75 kV. Electron microscope negatives were contact-reversed and printed as negative images.

Results

Overall Morphology of Subaxolemmal Cytoskeleton

When the axoplasm underlying the axolemma of the squid giant axon was chemically fixed by intraaxonal perfusion with the fixative containing 0.5% tannic acid and observed by thin section electron microscopy, the morphological integrity of the axoplasm was found to be well preserved. In transverse section, it was clearly observed that the axoplasm, ~20 μm thick, remained intact under the axolemma after intraaxonal perfusion with the SIS (Fig. 1). The subaxolemmal cytoskeleton was characterized by parallel bundles of longitudinally oriented microtubules which appeared to be interconnected by slender strands (Figs. 1 and 2 *a*). Neurofilaments were also observed to run parallel to the microtubules, but nearer to the axolemma, the density of the microtubules seemed to become greater. Occasionally, some microtubules grazed along the cytoplasmic surface of the axolemma and attached laterally to the axolemma through slender strands in a side-to-membrane fashion (Fig. 2, *a* and *b*). Furthermore, careful observations revealed that another type of filamentous structure ~4–5 nm in thickness was associated with the axolemma, and that these structures tangled with each other, forming spot-like clusters just beneath the axolemma (Figs. 1 and 2, *a* and *c*). Judging from their morphological characteristics and the biochemical data shown in the preceding paper (15), it appeared reasonable to consider that these clusters were mainly composed of actin filaments (microfilaments). Therefore, we could tentatively divide the axolemma into two domains: microtubule associated and microfilament associated.

To analyze the association of the subaxolemmal cytoskeletons with the cytoplasmic surface of the axolemma by the

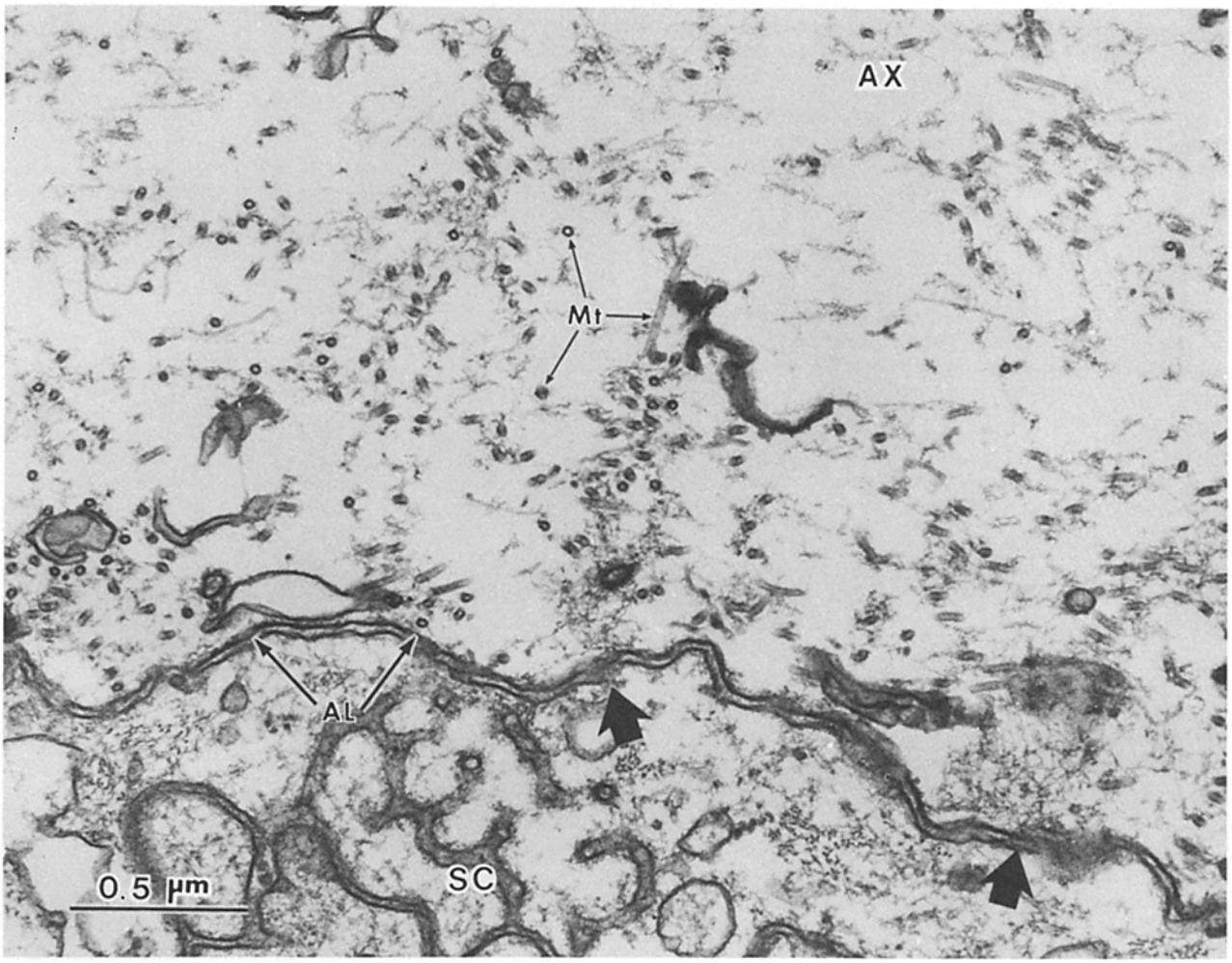

Figure 1. Transverse section of the subaxolemmal axoplasm of a squid giant axon. After intraaxonal perfusion with the SIS, the giant axon was fixed intraaxonally using the fixative containing 0.5% tannic acid. The giant axon is surrounded by a few layers of Schwann cells (*SC*). The subaxolemmal axoplasm (*AX*) is mainly composed of longitudinally oriented microtubules (*Mt*) and neurofilaments which are interconnected by slender strands. Thin filaments ~4–5 nm in thickness are associated with the axolemma (*AL*) and tangle with each other, forming spot-like clusters (large arrows).

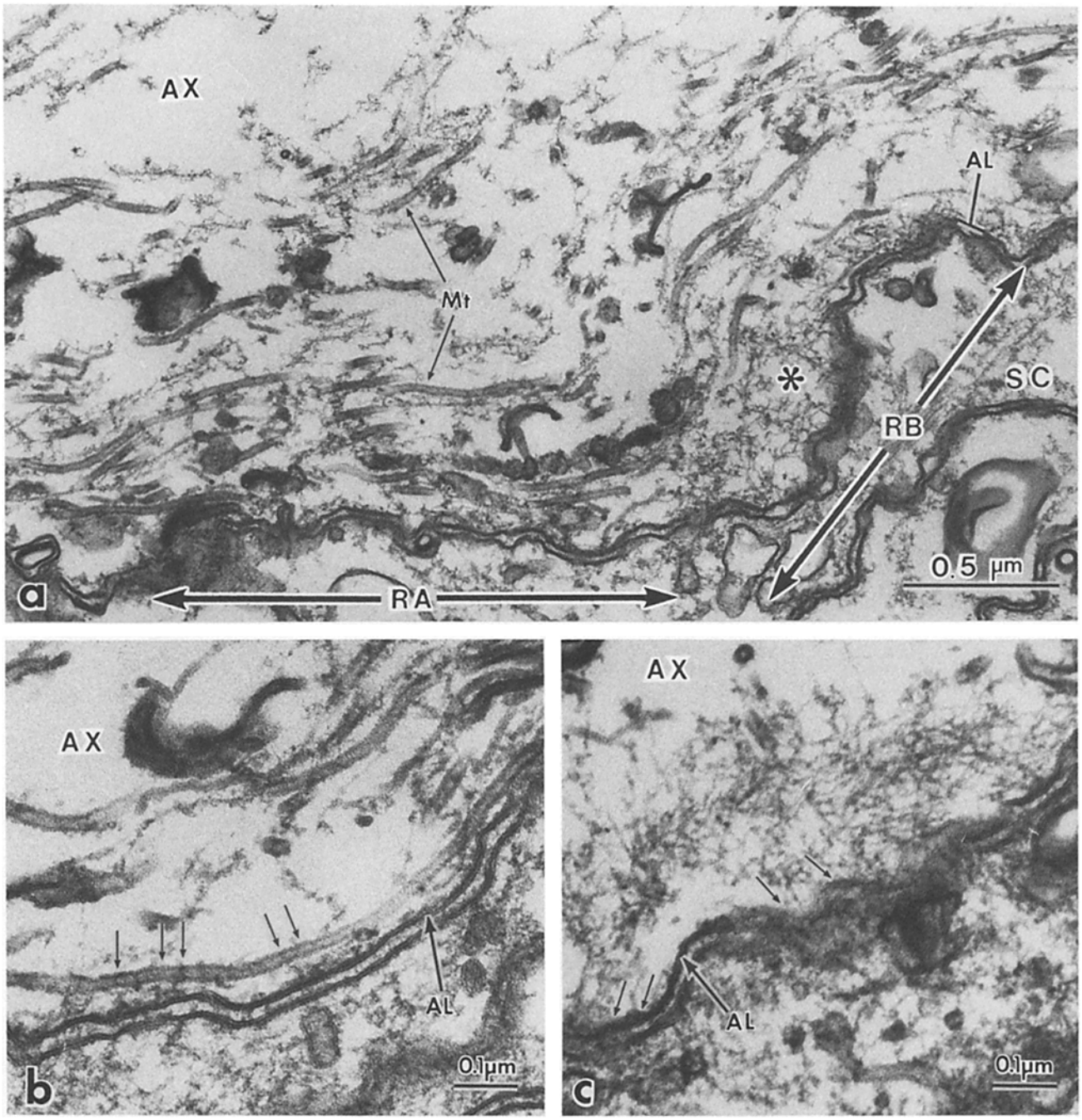

Figure 2. Longitudinal sections of the subaxolemmal cytoskeleton of a squid giant axon. (*a*) The axolemma (*AL*) of a giant axon is divided into two domains: microtubule associated (*RA*) and microfilament associated (*RB*). Microtubules (*Mt*) are oriented longitudinally, and some are associated laterally with axolemma. Microfilaments ~4–5 nm in thickness form spot-like clusters (*) just beneath the axolemma. *SC*, Schwann cell. (*b*) Microtubule-associated domain. One microtubule is seen to graze along the cytoplasmic surface of the axolemma (*AL*) and to attach laterally to the axolemma through slender strands (arrows) in a side-to-membrane fashion. (*c*) Microfilament-associated domain. Microfilaments (arrows) are seen to be associated with the axolemma (*AL*), forming spot-like clusters. *AX*, subaxolemmal axoplasm.

use of freeze-etch replica technique, some improvements in the preparation of the giant axon were required. Since the diameter of the giant axon was far larger than the depth of the samples frozen without ice-crystal formation, the cytoplasmic surface of the axolemma was not observable when the axon was rapidly frozen by touching its outer surface against a cooled copper block. Therefore, we have tried to develop a new preparation method to freeze the "opened" axon by touching its inner surface against the copper block, thus permitting direct observation of the cytoplasmic surface of the axolemma in deep-etch replica images (see Materials and Methods for details). With this preparation method, when the subaxolemmal cytoskeleton was fractured tangentially just beneath the axolemma, the cytoplasmic surface of both microtubule-associated and microfilament-associated domains of the axolemma was clearly observed (Fig. 3). The replicas also provided three-dimensional views of the well-developed cytoskeletal network underlying the axolemma, in which the

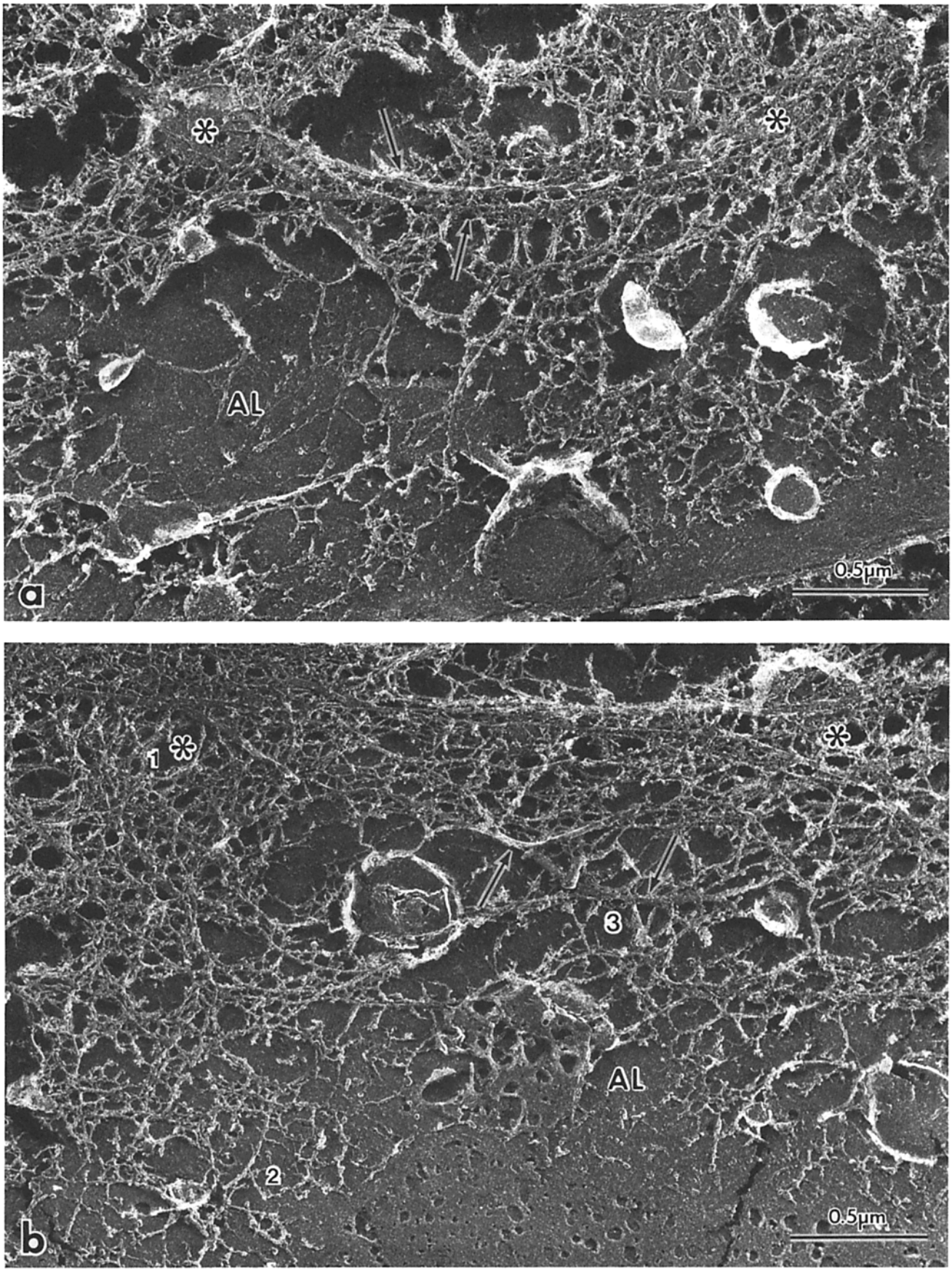

Figure 3. Freeze-etch replicas of the subaxolemmal cytoskeleton which is tangentially fractured just beneath the axolemma. The giant axon was intraaxonally fixed using chemical fixatives before rapid freezing. The subaxolemmal cytoskeleton was rapidly frozen by touching its inner surface against the copper block, thus permitting direct observation of the cytoplasmic surface of the axolemma (*AL*) in replica images. The replicas provide three-dimensional views of the well-developed cytoskeletal network underlying the axolemma, in which the microtubules (arrows) grazing along the axolemma and the clusters of microfilaments (•) are easily identified. The regions *1*, *2*, and *3* in *b* correspond to Figs. 6 *a*, 7, and 8, respectively.

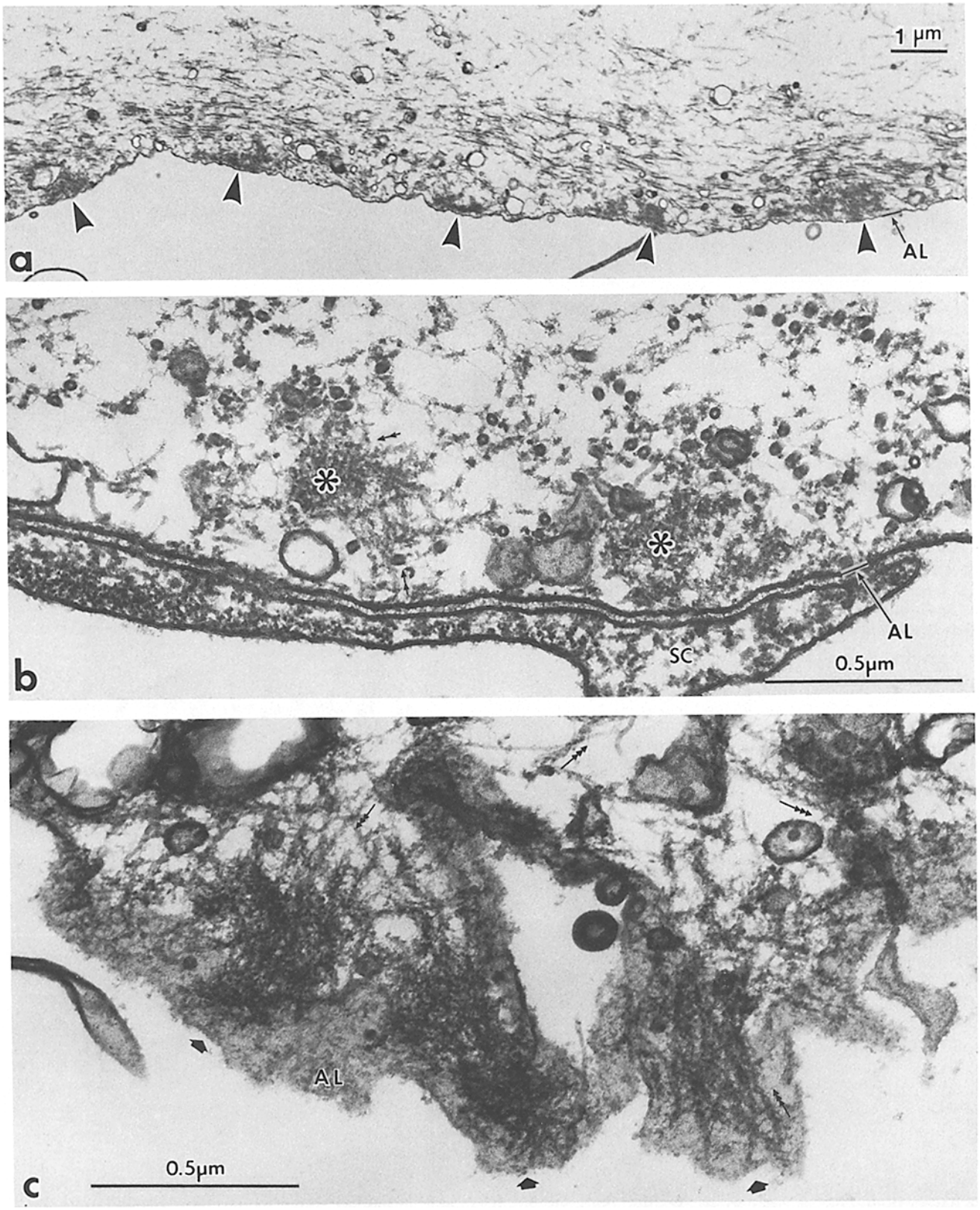

Figure 4. Subaxolemmal cytoskeleton of a giant axon after intraaxonal perfusion of HMM. (*a*) Longitudinal section. Electron-dense structures (arrowheads) are aligned just beneath the axolemma (*AL*). The axolemma is detached from the Schwann cells. (*b*) Transverse section. Note that the electron-dense structures (*) contain large number of actin filaments decorated with arrowheads of HMM (arrows). *SC*, Schwann cell. (*c*) Tangential section. Spot-like clusters (large arrows) of actin filaments decorated with arrowheads of HMM (small arrows) are clearly identified just beneath the axolemma (*AL*).

microtubules grazing along the axolemma and the clusters of microfilaments were easily identified. In the following sections, we describe the detailed morphology of the subaxolemmal cytoskeleton underlying the microfilament-associated and microtubule-associated domains of the axolemma.

Subaxolemmal Cytoskeleton Underlying the Microfilament-associated Domain of the Axolemma

To clarify the nature of the microfilament-like structures associated with the axolemma, HMM obtained from rabbit skeletal muscle was intraaxonally perfused before chemical fixation. As a result, large electron-dense structures were observed to be aligned just beneath the axolemma, often in a periodic manner (Fig. 4). The axolemma tended to be detached from the plasmalemma of the surrounding Schwann cells. At higher magnification, these electron-dense structures were seen to contain a large number of microfilaments decorated with arrowheads of HMM, indicating that the clusters of microfilament-like structures seen in nontreated axoplasm mainly consisted of actin. These microfilaments were seen to

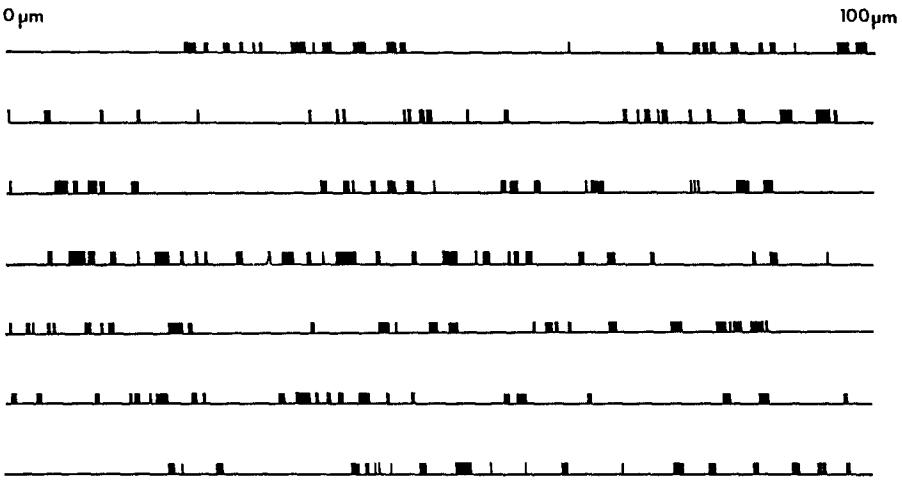

Figure 5. Distribution of the microfilament clusters along the axolemma half round the axon. The microfilament-associated domains are marked. Approximately 15% of the axolemma is associated with the microfilament clusters.

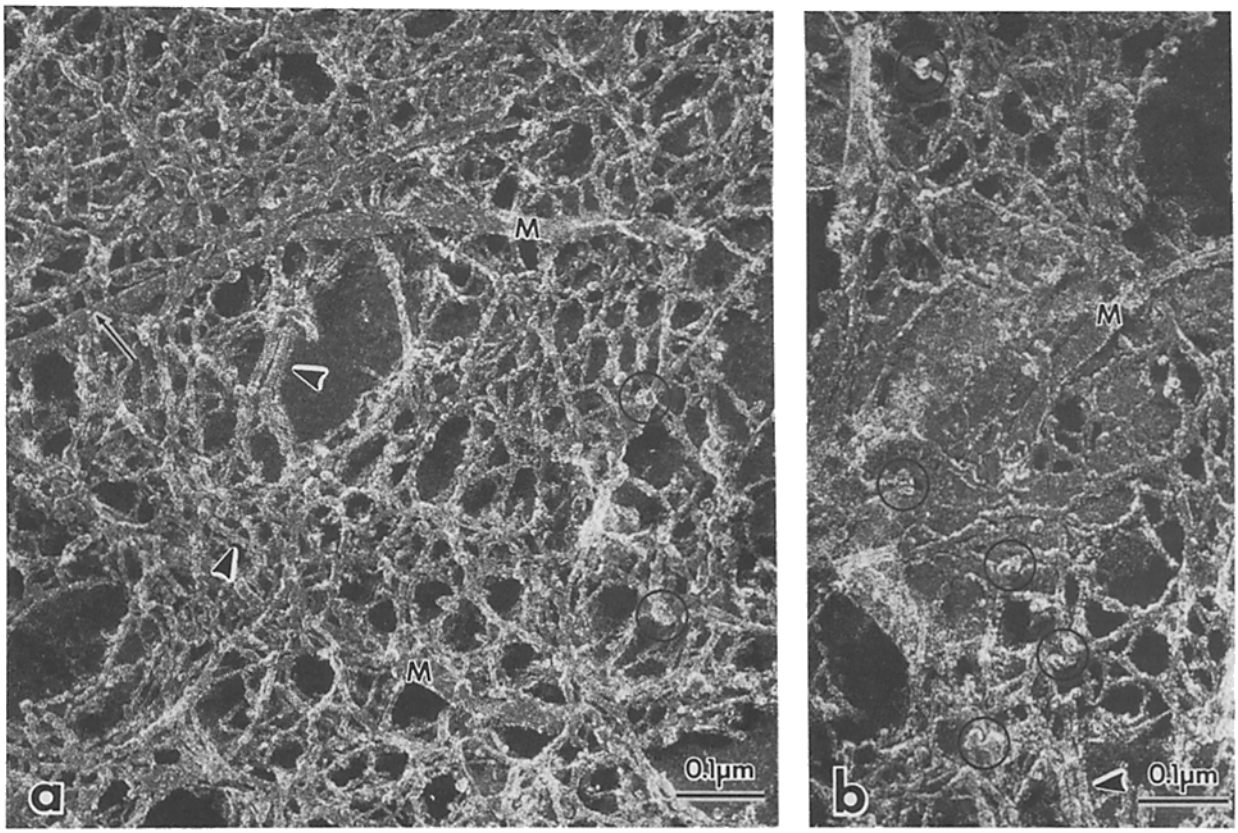

Figure 6. Freeze-etch replicas of microfilament clusters just beneath the axolemma. *a* corresponds to the region *1* in Fig. 3 *b*. Some microfilaments show ~5 nm a period on their surface (arrowheads), which may correspond to the pitch of the genetic helix of actin filament. Microfilaments are intertangled, forming a complicated three-dimensional network together with thin cross-linking strands. Globular structures ~30–35 nm in diameter showing a horseshoe-like appearance are encircled. Some microtubules (*M*) are observed to run into the microfilament clusters and to be associated with microfilaments through short slender strands (arrow).

be associated with the axolemma (see Fig. 2*c*), but after HMM treatment, most of the microfilaments were detached from the axolemma. Therefore, it was not possible to determine the polarity of microfilaments with respect to the axolemma.

The question naturally arose of what percentage of the axolemma was covered with the clusters of microfilaments. To answer this question, in transverse sections, we have traced the axolemma half round the axon. The details on the distribution of the microfilament clusters along the axolemma are shown in Fig. 5. Five different axons were analyzed, and it became clear that 15 ± 5% (± SD) of the axolemma was associated with the microfilament clusters.

Next, using rapid-freeze, deep-etch replica electron microscopy, we analyzed the ultrastructure of the cytoplasmic surface of the microfilament-associated domains of the axolemma and the underlying microfilament clusters (Fig. 6). For this purpose, the giant axon was intraaxonally perfused with the SIS to wash out the soluble proteins before chemical fixation. Furthermore, the samples were washed with distilled water just before rapid freezing, thus excluding the possibility that soluble proteins and salts might produce artifactual structures during freezing and etching. In such replica images, the microfilament cluster seen in thin section electron microscopy was easily identified as a complicated three-dimensional network in which microfilaments were intertangled. Some microfilaments showed ~5 nm a period on their surface, which might correspond to the pitch of the genetic helix of actin filaments (7). Within the network of microfilaments, thin

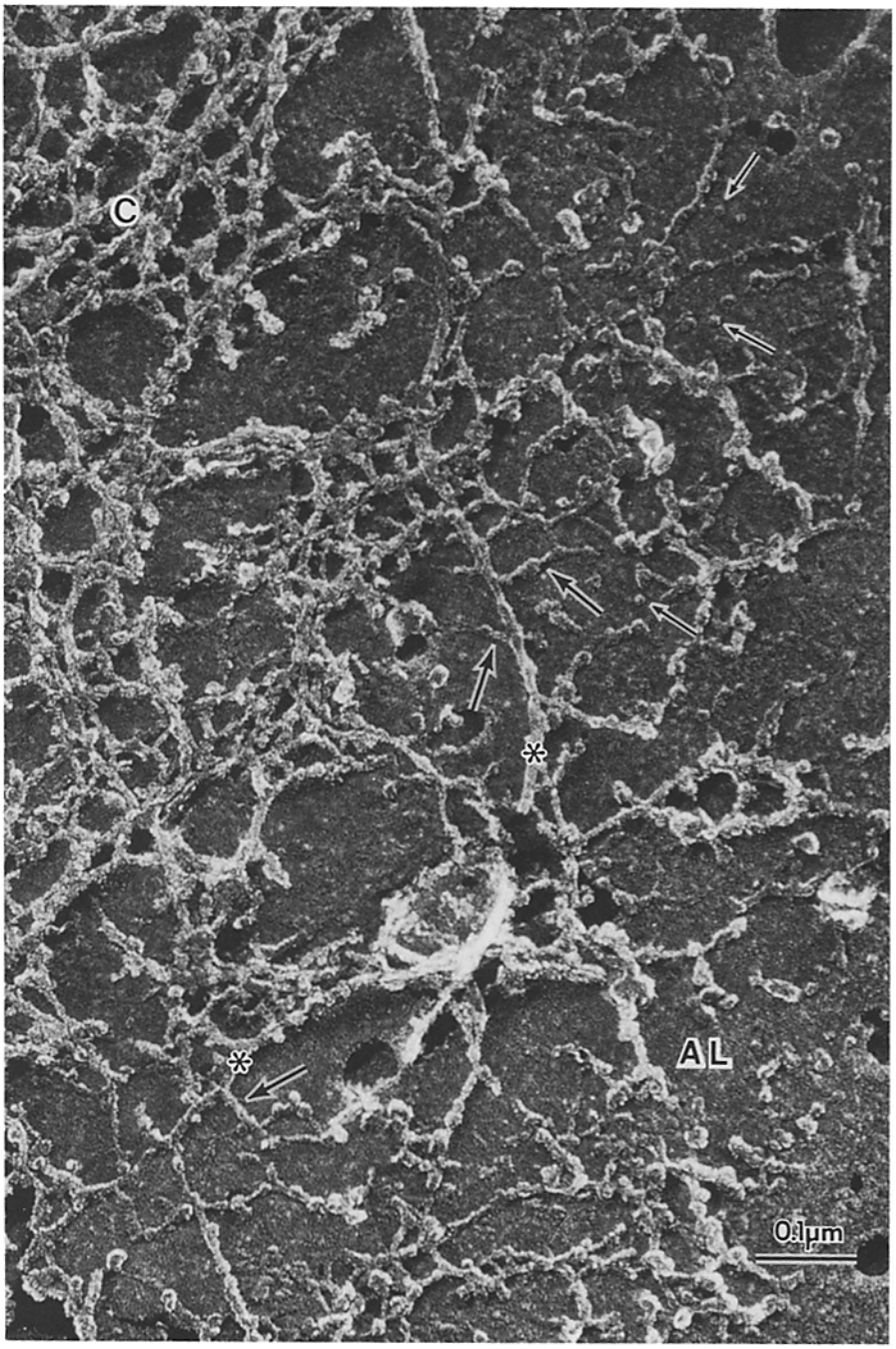

Figure 7. Freeze-etch replica of the specialized layer of the meshwork of thin strands identified between the microfilament clusters and the axolemma. This image is a high-power electron micrograph from the region *2* in Fig. 3*b*. Note a large number of globular extrusions ~5–10 nm in diameter (small arrrows) on the cytoplasmic surface of the axolemma (*AL*), some of which are associated with the meshwork of thin strands (large arrows). Microfilaments (*) are seen to run parallel to this meshwork and to be associated with thin strands. *C*, clusters of microfilaments.

cross-linking strands and globular structures were distributed. Some globular structures ~30–35 nm in diameter showed a characteristic horseshoe-like appearance which resembled the molecular shape of the 255-kD protein described in the preceding paper (15). Occasionally, some microtubules were observed to run into the microfilament clusters and to be intermingled with microfilaments in a complicated manner.

A specialized layer of the characteristic meshwork of thin strands was identified between the microfilament clusters and the axolemma (Fig. 7). This meshwork of thin strands was directly applied to the cytoplasmic surface of the axolemma. Careful observations revealed that many globular extrusions ~5–10 nm in diameter occurred on the cytoplasmic surface of the axolemma, and some of them were associated with the meshwork of thin strands. Microfilaments ran parallel to this meshwork and associated laterally with it, thus being incorporated into the meshwork itself. These observations revealed that microfilaments in the clusters did not bind to the cytoplasmic surface of the axolemma directly, but through a two-dimensional meshwork of thin strands just beneath the axolemma.

Subaxolemmal Cytoskeleton Underlying the Microtubule-associated Domains of the Axolemma

In both thin section and freeze-etch replica electron microscopy, it was clear that among the clusters of microfilaments the longitudinally oriented microtubules grazed along and associated with the cytoplasmic surface of the axolemma (Figs. 2 and 3). When this association was carefully observed in the stereo pair micrographs of replicas, the microtubules were seen to be connected laterally on the cytoplasmic surface by slender strands (Fig. 8). Some microfilaments extended out from the neighboring clusters and ran closely with the microtubules associated with axolemma, forming a complicated coarse network around microtubules held together with slender strands.

The bundles of microtubules associated with the axolemma were seen to be pushed away from the axolemma at the microfilament-associated domains (see Fig. 2). Therefore, when the axoplasm of the chemically fixed giant axon was fractured tangentially at some distance from the axolemma, the replicas obtained were characterized only by the longitudinally oriented microtubules (Fig. 9 *a*). Interestingly, these microtubules were embedded in a well-developed, three-dimensional fine meshwork. When compared to the chemically fixed axons, this meshwork appeared to be denser in the replicas obtained from the unfixed axons which were intraaxonally perfused with the SIS before freezing (Fig. 9 *b*). This difference may be partly because the morphological integrity of the fine meshwork was not completely preserved by chemical fixation and partly because the salts in the SIS were deposited on the original meshwork during etching of the unfixed axons. In both cases, this fine meshwork was composed of rod structures ~5 nm in thickness and granular structures ~5–10 nm in diameter. The outer surfaces of the microtubules were rather smooth, showing the arrangements of tubulin subunits. Some of the rod structures from the meshwork attached to the surface of the microtubules at various angles without any definite periodicity.

Considering that the axolinin was the major microtubule-

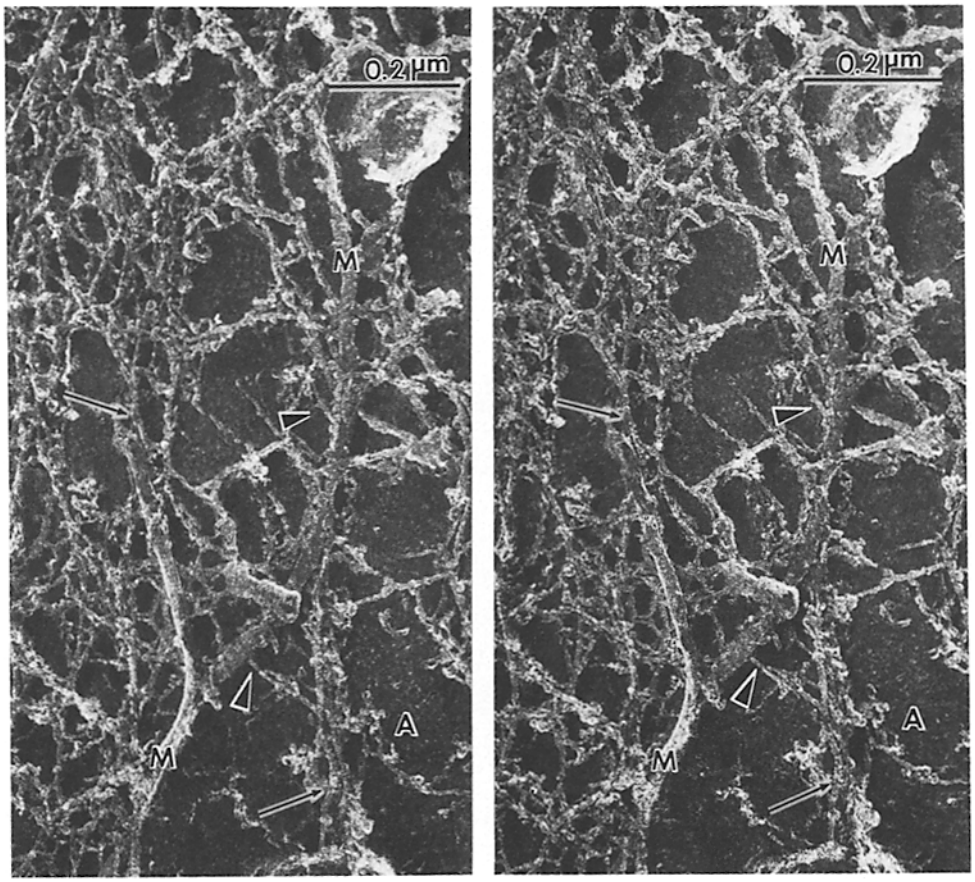

Figure 8. Stereo pair micrographs of freeze-etch replica of the microtubule-associated domain of the axolemma. This image corresponds to the region *3* in Fig. 3 *b*. Two microtubules (*M*) are seen to graze along the cytoplasmic surface of the axolemma (*A*) and to be connected laterally to the axolemma by slender strands (arrowheads). Some microfilaments (arrows) extend out from the neighboring clusters and run closely with the microtubules.

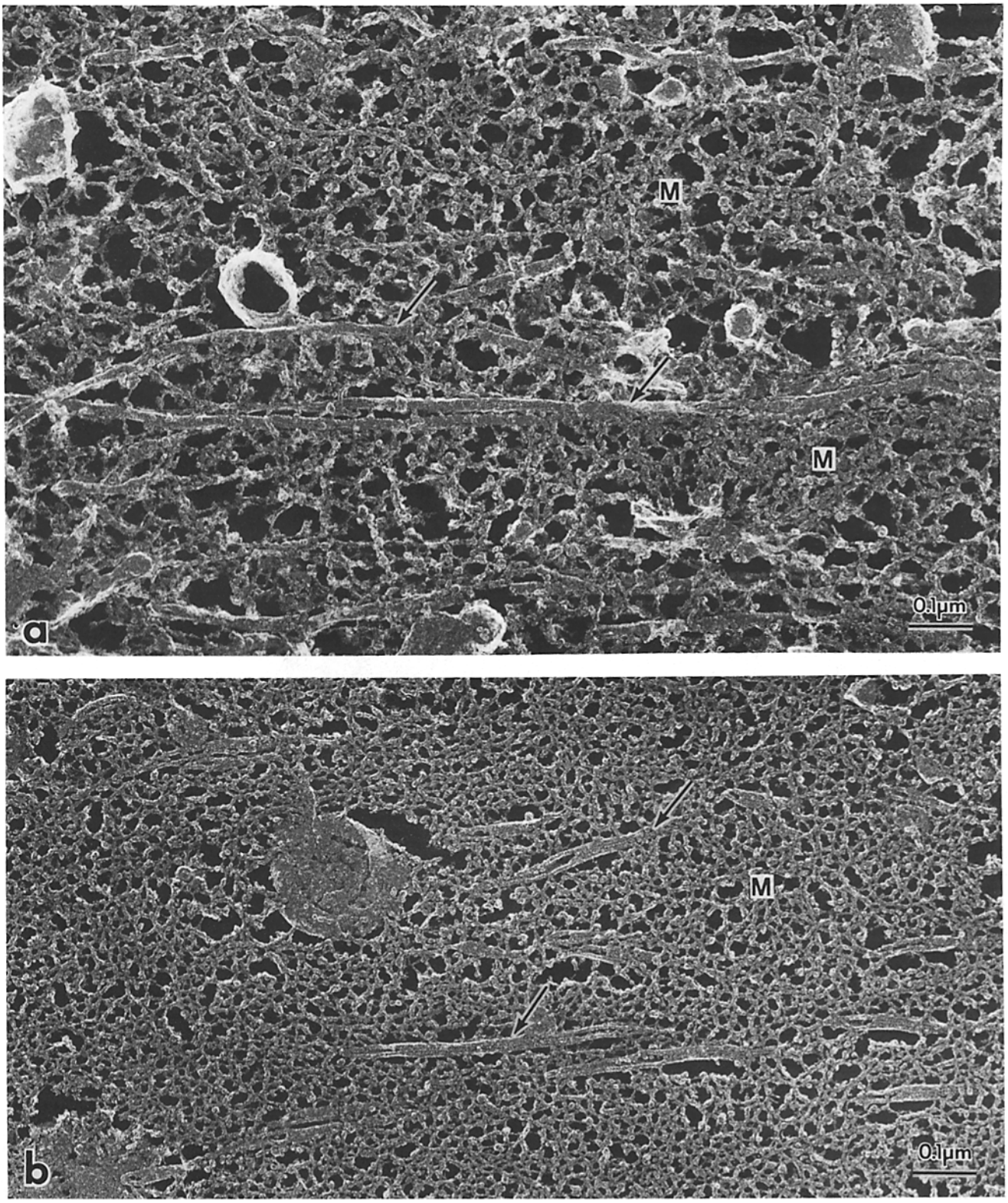

Figure 9. Freeze-etch replicas of the subaxolemmal axoplasm which is fractured tangentially at some distance from the axolemma. (*a*) Chemically fixed subaxolemmal axoplasm. The fixative was washed out by distilled water containing 10% methanol before rapid freezing. The replica is characterized by the longitudinally oriented microtubules (arrows), which are embedded in a well-developed, three-dimensional fine meshwork (*M*). (*b*) Unfixed subaxolemmal axoplasm. Note that the fine meshwork (*M*) among microtubules (arrows) is denser when compared to that in chemically fixed axoplasm.

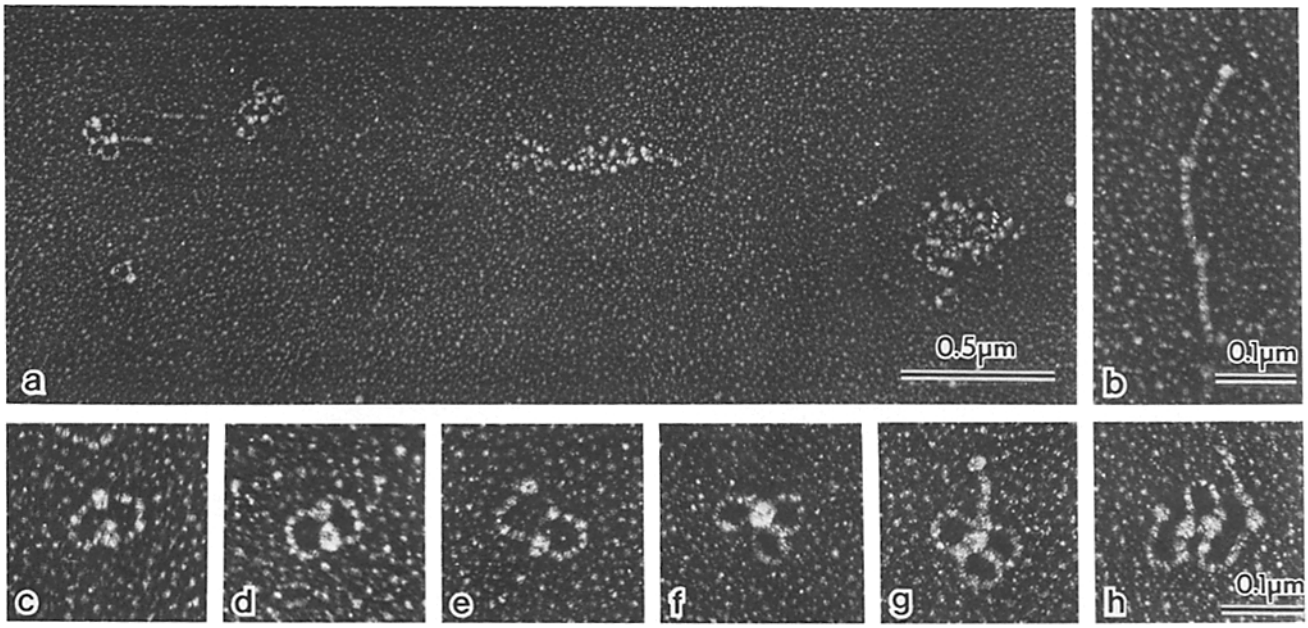

Figure 10. Morphology of the aggregates of the axolinin molecules in 0.1 M NaCl solution in rotary-shadowed preparations. In 0.1 M NaCl solution, the axolinin molecules form various sizes of aggregates (*a*). Two (*c–e*), three (*b* and *f*), or four (*g* and *h*) molecules form small aggregates by a head-to-tail association between two molecules.

associated protein highly enriched in the subaxolemmal cytoskeleton and that the axolinin molecule looked like a straight rod ~105 nm in length with a globular head at one end (15), we were led to speculate that the fine meshwork surrounding the microtubules might be mainly composed of axolinin. To verify this speculation, we have analyzed the ultrastructure of the aggregates formed in vitro by axolinin alone. When the axolinin in 0.6 M NaCl solution was dialyzed against 0.1 M NaCl solution, the axolinin precipitated as large aggregates. Then, at first, the aggregation pattern of the axolinin molecule in 0.1 M NaCl solution was analyzed using the low-angle rotary-shadowing method. Even if the 0.6 M NaCl solution containing axolinin was diluted into 0.1 M NaCl solution as quickly as possible before being sprayed onto mica, almost all axolinin was incorporated into large aggregates (Fig. 10). Small aggregates which consisted of 2–4 molecules of axolinin were used to analyze how the axolinin molecules formed aggregates. As shown in Fig. 10, the axolinin molecules were seen to be successively incorporated into aggregates by a head-to-tail association between two molecules, and each molecule in the aggregates tended to form a ring structure. Furthermore, the large aggregates of axolinin dialyzed against distilled water were observed by the rapid-freeze, deep-etch replica electron microscopy (Fig. 11). Most interestingly, the aggregates of the purified axolinin bore a morphological resemblance to the in vivo fine meshwork surrounding microtubules (see Fig. 9); it looked like a complicated three-dimensional meshwork mainly consisting of rod structures and granular structures.

Next, using the low-angle rotary-shadowing method, the mode of association of the axolinin molecule to tubulin was examined in vitro (Fig. 12). When the purified tubulin was mixed with 0.6 M NaCl and 50% glycerol for low-angle rotary-shadowing electron microscopy, small round aggregates of tubulin were observed. On the other hand, the electron microscopic image obtained from a mixture of the axolinin and purified tubulin under the same conditions was characterized by spider-like structures consisting of the aggregates of tubulin and several axolinin molecules. In these complexes, each

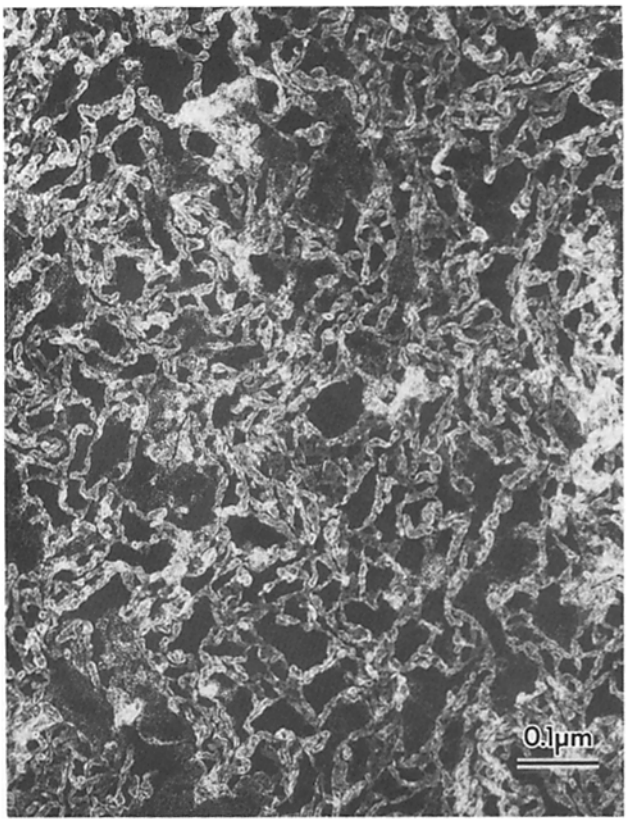

Figure 11. Freeze-etch replica of the aggregates of the axolinin molecules in distilled water containing 0.1 mM EDTA (pH 7.0). The replica is characterized by three-dimensional fine meshwork, which resembles the in vivo meshwork seen in Fig. 9*a*.

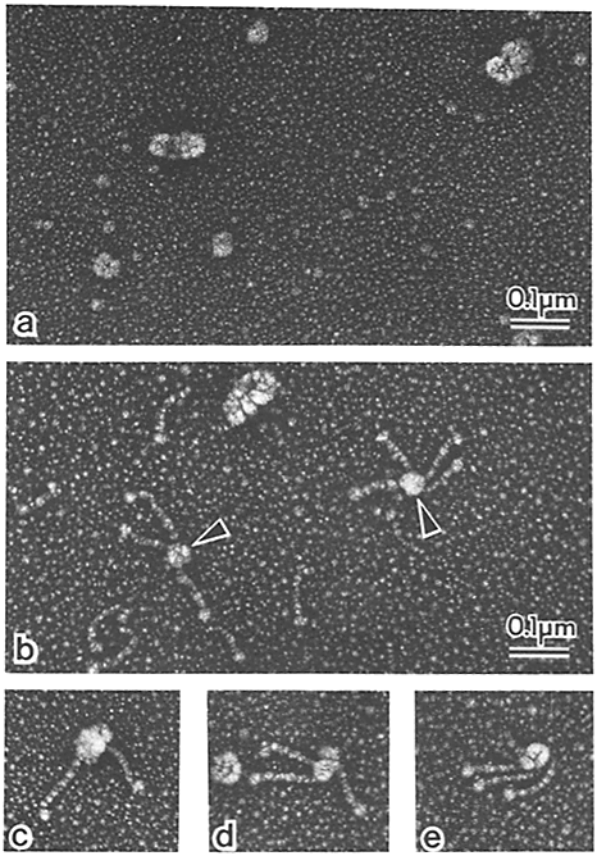

Figure 12. Rotary-shadowing electron micrographs of axolinin–tubulin complexes. (*a*) Purified tubulin forms small aggregates in a 0.6 M NaCl solution containing 50% glycerol. (*b–e*) The mixture of axolinin and purified tubulin in the same condition. Each axolinin molecule is associated with a tubulin aggregate (arrowheads) at its tail end, forming spider-like structures.

axolinin molecule was associated with a tubulin aggregate at its tail end, indicating that a tubulin-binding site was located at the tail end of the axolinin molecule. These observations in vitro appeared to favor the idea that in the subaxolemmal cytoskeleton, the microtubules were embedded in the fine meshwork mainly consisting of axolinin molecules and associated with this meshwork at the free tail ends of the axolinin molecules.

To further confirm this idea, using the anti-axolinin antibody described in the preceding paper (15), we analyzed the localization of the axolinin in squid giant axon at both light and electron microscopic levels. Indirect immunofluorescence microscopy revealed that, in both transverse and longitudinal frozen sections of squid nerves containing a giant axon, intense fluorescence appeared at the periphery of the axoplasm of a giant axon (Fig. 13). Weaker staining was also detected in the central region of the axoplasm in the giant axon. A similar distribution pattern of the axolinin was observed in the intermediate-sized axons surrounding the giant axon. In small axons, however, the axoplasm was homogeneously stained. Then, the localization of the axolinin molecule in the subaxolemmal cytoskeleton of a giant axon was analyzed at the electron microscopic level using the immunogold method. During this analysis, we faced a technical problem: the microtubule in the subaxolemmal cytoskeleton

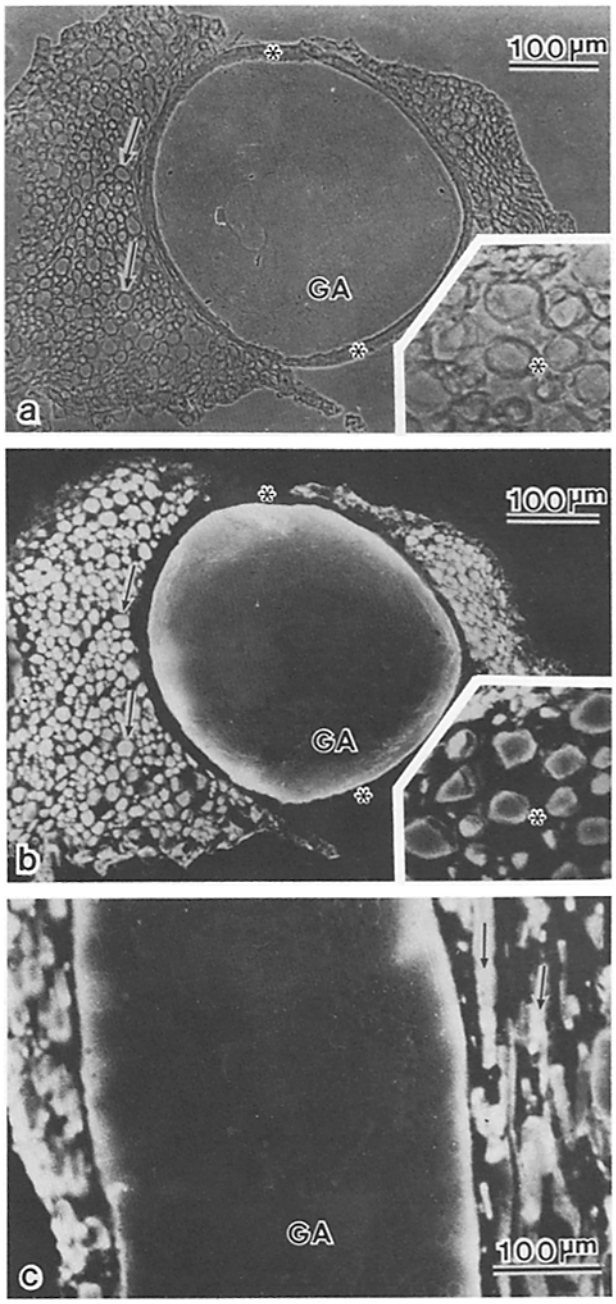

Figure 13. Immunofluorescence microscopic localization of the axolinin in frozen sections of the squid nerve containing a giant axon. (*a*) Phase-contrast micrograph of a transverse frozen section. A giant axon (*GA*) is surrounded by Schwann cells (*) and bundles of intermediate-sized and small axons (arrows). (*Inset*) Higher magnification of intermediate-sized and small axons. Each axon is also surrounded by Schwann cells (*). (*b*) Indirect immunofluorescence micrograph of the same transverse frozen section. Intense fluorescence appears at the periphery of a giant axon (*GA*) and intermediate-sized axons (*inset*). In small axons (*inset*), the axoplasm is homogeneously stained. Note that Schwann cells (*) are not stained. (*c*) Indirect immunofluorescence micrograph of a longitudinal frozen section. Intense staining is detected at the periphery of the axoplasm of a giant axon (*GA*).

was highly unstable even if the axoplasm was intraaxonally perfused with 0.5% glutaraldehyde for 10 min. To solve this problem, we used a solution containing 95 mM potassium glutamate for almost all steps (see Materials and Methods for

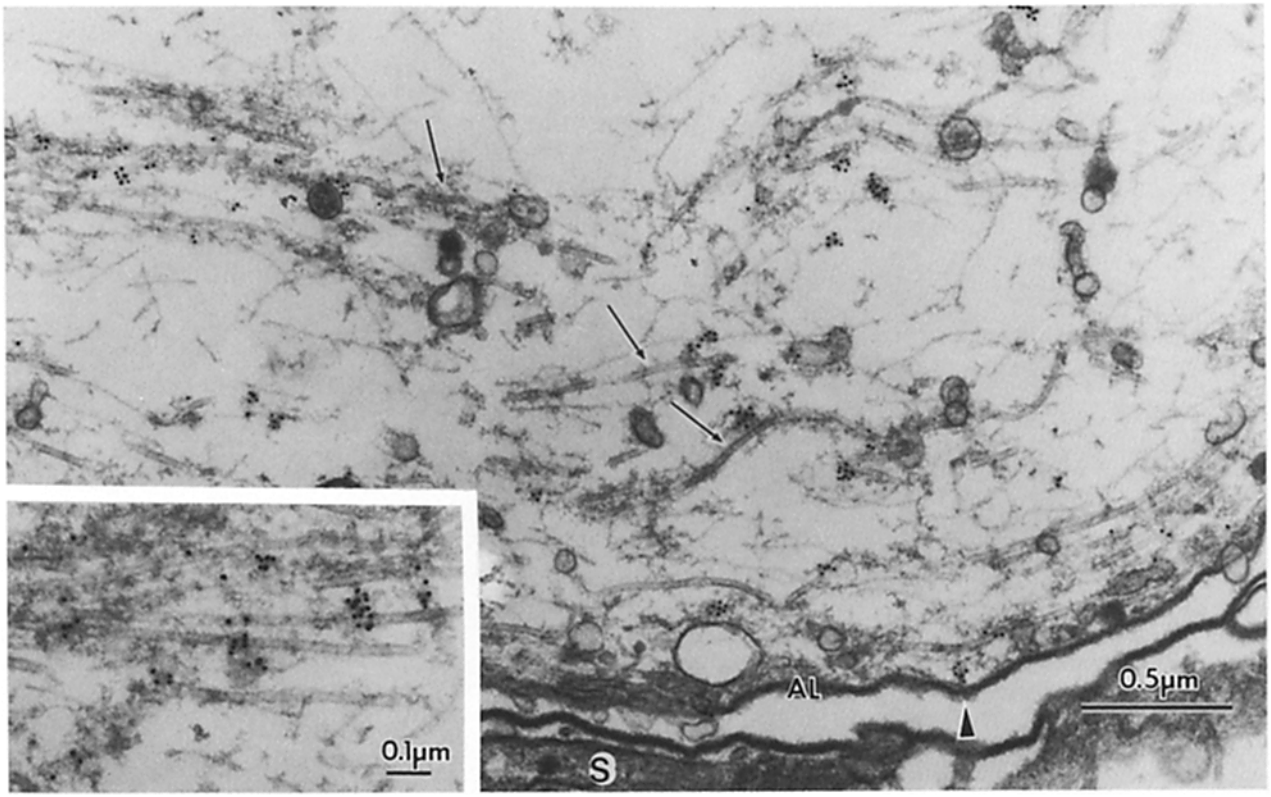

Figure 14. Immunogold labeling pattern of axolinin in the subaxolemmal cytoskeleton of a squid giant axon. The sample was first treated with anti-axolinin antibody followed by secondary antibody coupled with 10-nm gold. The fine meshwork surrounding the microtubules (arrows) are specifically labeled. Note that axolinin immunolabeling is absent or very low in the neurofilament-rich region. The slender strands (arrowheads) connecting the microtubules to the axolemma (*AL*) are also immunolabeled, but only on rare occasions. *S*, Schwann cell.

details). This solution had the remarkable effect of preserving the microtubules during antibody labeling. As a result, the slender strands surrounding the microtubules in the subaxolemmal cytoskeleton were specifically labeled (Fig. 14). Axolinin immunolabeling was absent or very low in the neurofilament-rich region. The slender strands connecting the microtubules to the axolemma were also immunolabeled, but only on rare occasions. The shorter the prefixation time, the larger was the amount of labeled gold, although prefixation with 0.5% glutaraldehyde for more than 10 min was required for the preservation of microtubules. When the sample was incubated with non-immune IgG instead of the anti-axolinin antibody, no structures in the subaxolemmal cytoskeleton were immunolabeled.

Taking these findings together, we concluded that the subaxolemmal cytoskeleton underlying the microtubule-associated domains of axolemma, which was pushed away from the axolemma at the microfilament-associated domains, was mainly composed of the longitudinally oriented microtubules embedded in the fine meshwork mainly consisting of the axolinin.

Discussion

In the preceding paper, we have demonstrated biochemically that the subaxolemmal cytoskeleton of the squid giant axon is highly specialized, and that it is mainly composed of tubulin, actin, and two unique high-molecular-weight proteins (axolinin and the 255-kD protein) (15; see also 25, 29, 30). Therefore, in this paper, we have attempted to morphologically analyze how these proteins are organized into the subaxolemmal cytoskeletons in situ. The results indicated that the major constituents of the subaxolemmal cytoskeleton of the squid giant axon were microtubules and microfilaments (actin filaments). The microfilaments appeared to be associated with the axolemma through a specialized meshwork of thin strands, forming spot-like clusters just beneath the axolemma. The microtubules ran parallel to the axolemma and embedded in the fine meshwork mainly consisting of the axolinin. Some microtubules grazed along the axolemma among the clusters of microfilaments and associated laterally with the axolemma through slender structures. Therefore, the axolemma could be divided into microfilament-associated and microtubule-associated domains (Fig. 15).

Recently the biochemical and morphological aspects of the axonal cytoskeleton of the squid giant axon were intensively studied by Lasek and his colleagues (21, 23, 24). Their studies were mainly focused on the axonal cytoskeleton of the extruded axoplasm (central part of the axoplasm). According to their morphological studies, the cytoskeleton of the extruded axoplasm was characterized by the longitudinally oriented microtubules and the neurofilament lattice, which were interconnected by slender strands. Our freeze-etch replica images of the chemically fixed extruded axoplasm also confirm their observations (Fig. 16). A comparison of Fig. 16 and Fig. 9 renders strong support to the idea that the cytoskeleton of a

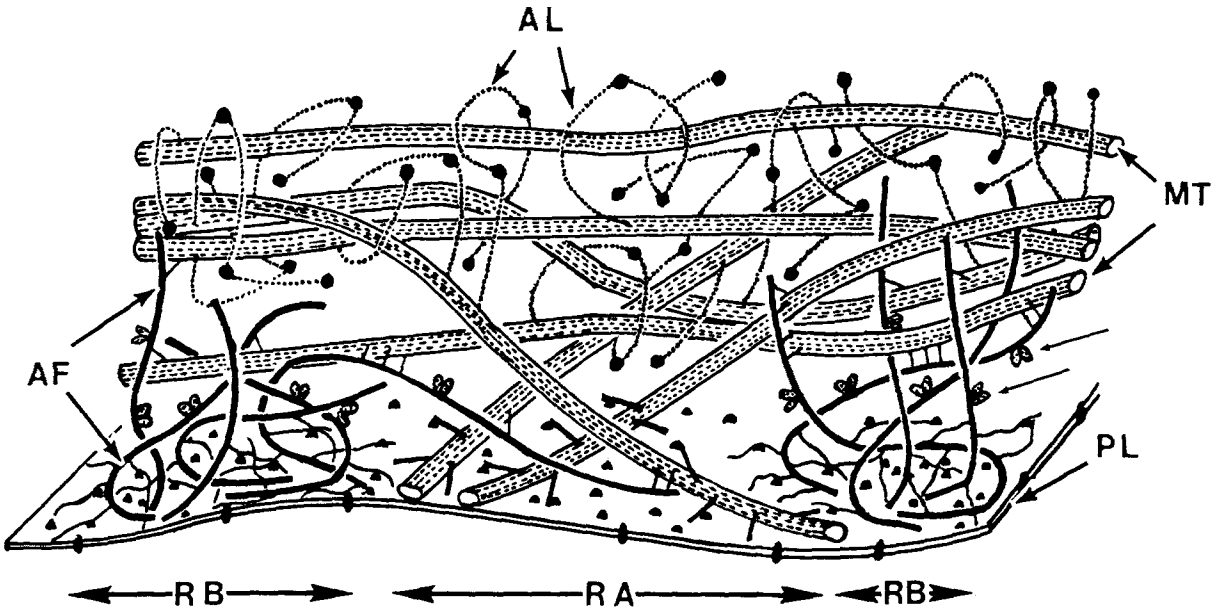

Figure 15. Schematic drawing of the architecture of the subaxolemmal cytoskeleton of a squid giant axon. The plasmalemma (*PL*) of a giant axon can be divided into two domains, microtubule associated (*RA*) and microfilament associated (*RB*), and the subaxolemmal cytoskeleton is mainly composed of spot-like clusters of microfilaments (*AF*) and longitudinally oriented microtubules (*MT*), which are embedded in the fine meshwork mainly consisting of axolinin (*AL*). The horseshoe-shaped structures (small arrows) on the microfilaments may be the morphological counterparts of the 255-kD protein. Note three different types of cross-linkers between (*a*) MT and AF, (*b*) MT and PL, (*c*) AF and PL. See details in the text.

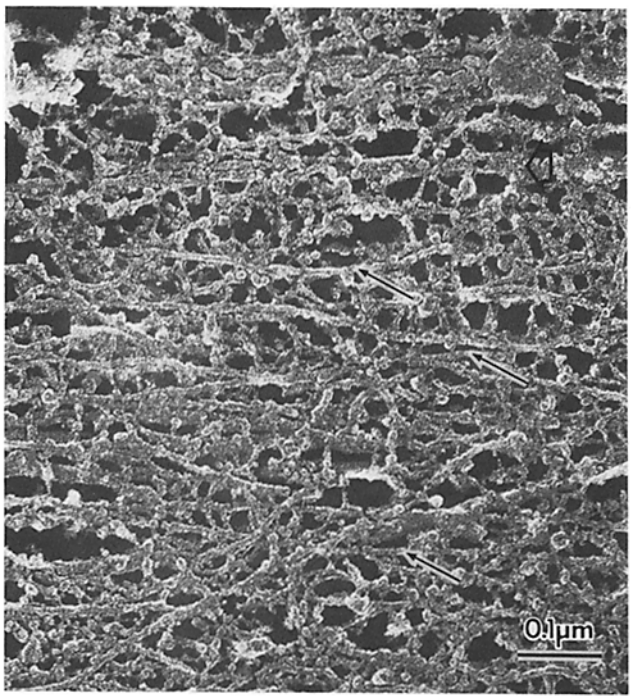

Figure 16. Freeze-etch replica of the extruded axoplasm of a squid giant axon. The axoplasm was chemically fixed and washed with distilled water before freezing. Note that the longitudinally oriented neurofilaments (small arrows) are merely connected with each other by thin strands, showing a ladder-like appearance. The fine meshwork surrounding microtubules (large arrow) are not well developed when compared to that in Fig. 9*a*.

squid giant axon is specialized into the peripheral and central portions.

The morphology of the subaxolemmal cytoskeleton of the squid giant axon was first analyzed in detail by Metuzals and Tasaki using scanning electron microscopy (22). They successfully visualized the three-dimensional cytoskeletal network underlying the axolemma. However, probably because pronase was used in the perfusion solution and because the giant axon was prefixed from the outside, the microtubules were not identified in large amounts in their micrographs. As shown in the present study, use of the roller method, instead of the pronase method, and intraaxonal perfusion with fixative that contained tannic acid were very effective in preserving the morphology of the subaxolemmal cytoskeleton, especially microtubules and microfilaments.

Our in vitro observations on the aggregates of axolinin and in situ immunoelectron microscopic analysis have led us to conclude that in the subaxolemmal cytoskeleton the parallel bundles of microtubules are embedded in the fine meshwork mainly consisting of the axolinin molecules. As shown in the preceding paper (15), axolinin accounted for almost 9% of the total protein in the subaxolemmal cytoskeleton, and tubulin for only 8%. Therefore, it may be reasonable to consider that the majority of the thin strands seen in Fig. 9*a* are composed of axolinin molecules. The axolinin molecule was shown to form large aggregates by a head-to-tail association and to bind to a microtubule at its tail end in vitro. Therefore, the axolinin molecule appeared not to work as a simple cross-linker between two microtubules, but to entangle the microtubules in the aggregates of axolinin. This microtubule–axolinin meshwork underlying the axolemma was reported to play a crucial role in the excitation of the axolemma (19, 20), but the detailed mechanism remains to be elucidated in molecular terms. However, it is interesting to point out the morphological resemblance of this meshwork to the axoplasm of the nodal part of the mammalian myelinated axons, in which microtubules were enriched and appeared to be em-

bedded in the three-dimensional fine meshwork (32).

Biochemical and immunological analyses argue strongly for the existence of a large amount of actin inside mammalian axons (2, 13, 16, 31, 40) as well as inside squid giant axon (22, 24, 29). Our preceding paper also clearly demonstrated that actin was one of the major constituents of the subaxolemmal cytoskeleton of squid giant axons (15). However, the electron microscopic studies in which actin filaments were clearly visualized inside axons were the exception. Such discrepancy may be partly due to the difficulty of the fixation of actin filaments in axoplasm and partly due to existence of nonfilamentous actin inside the axoplasm (24). In the squid giant axon, Metuzals and Tasaki (22) have shown that some of the filamentous structures in the subaxolemmal cytoskeleton were decorated with HMM using the "glycerinated" axons. Our present observations revealed that a large number of HMM-decorated filaments appeared when HMM was "intraaxonally" perfused. Furthermore, without HMM treatment, in both thin section and replica images, the microfilaments were directly observed to form clusters just beneath the axolemma. Within these clusters, horseshoe-shaped granular structures appeared to be distributed, leading us to speculate that these were the morphological counterparts of the actin-binding 255-kD protein purified in the preceding study (15). It is still premature to discuss the physiological roles of these microfilament clusters, but, interestingly, such an arrangement of microfilaments is in excellent agreement with the model for the movement of the cytoskeleton in slow axonal transport proposed by Lasek and Hoffman (17). If myosin-like ATPase is, as postulated, associated with the cytoskeletal network inside axons, it is easy to explain the force generation for the slow axonal transport.

Together with the preceding paper, this study has given an outline of the molecular organization of the subaxolemmal cytoskeleton in squid giant axons. Furthermore, in these studies, we have developed several techniques to analyze the subaxolemmal cytoskeleton biochemically and morphologically. In the next step, using these techniques, we must identify the proteins which connect microtubules and microfilaments to the axolemma. In the microtubule-associated domains, the microtubules were associated laterally with the axolemma through slender strands, which were not axolinin judging from the results of immunoelectron microscopy. In the microfilament-associated domains, a specialized meshwork of slender strands connected the microfilament clusters to axolemma. This meshwork strongly resembled the spectrin–actin network underlying the human erythrocyte membrane (3, 33, 35). Considering that spectrin-like proteins (fodrin or calspectin) are reported to localize just beneath the axolemma in mammalian axons (6, 14, 18, 28, 34), it may well be that the meshwork in the microfilament-associated domains is mainly composed of spectrin-like proteins and actin. Purification and characterization of the spectrin-like protein from squid giant axon will evaluate this speculation. Another problem to be settled is whether the sodium channels are located in the microtubule-associated or microfilament-associated domains of the axolemma. We believe that further studies on these problems will lead to better understanding of the physiological roles of the subaxolemmal cytoskeleton in membrane excitation.

We wish to thank Professors H. Sakai and M. Kurokawa (University of Tokyo) and Professor H. Ishikawa (Gunma University) for their helpful discussions and encouragement throughout this study, and Drs. M. Ichikawa, M. Urayama, and Y. Kawakami (Electrotechnical Laboratory, Tsukuba) for their collaboration on the intraaxonal perfusion. Thanks are also due to Dr. M. Yano (University of Tokyo) for his generous gift of heavy meromyosin obtained from rabbit skeletal muscle, and to Dr. T. Arai (Tsukuba University) for his helpful advice. Rapid freezing with liquid helium in the early stage of this study was carried out in the Cryogenic Center at the University of Tokyo.

This study was supported in part by research grants from the Ministry of Education, Science and Culture, Japan, and from the Mitsubishi Foundation.

Received for publication 22 July 1985, and in revised form 20 November 1985.

References

1. Baker, P. F., A. L. Hodgkin, and T. I. Show. 1962. Replacement of the axoplasm of giant nerve fibres with artificial solutions. *J. Physiol. (Lond.).* 164:330–354.

2. Black, M. M., and R. J. Lasek. 1979. Axonal transport of actin: slow component b is the principal source of actin for the axon. *Brain Res.* 171:401–413.

3. Branton, D., C. M. Cohen, and J. Tyler. 1981. Interaction of cytoskeletal proteins on the human erythrocyte membrane. *Cell.* 24:24–32.

4. Chan-Palay, V. 1972. The tripartite structure of the undercoat in initial segments of Purkinje cell axons. *Z. Anat. Entwicklungsgesch.* 139:1–28.

5. Endo, S., H. Sakai, and G. Matsumoto. 1979. Microtubules in squid giant axon. *Cell Struct. Funct.* 4:285–293.

6. Glenney, J. R., Jr., P. Glenney, M. Osborn, and K. Weber. 1982. An F-actin- and calmodulin-binding protein from isolated intestinal brush borders has a morphology related to spectrin. *Cell.* 28:843–854.

7. Heuser, J. E., and R. Cooke. 1983. Actin-myosin interactions visualized by the quick-freeze, deep-etch replica technique. *J. Mol. Biol.* 169:97–122.

8. Heuser, J. E., and M. W. Kirschner. 1980. Filament organization revealed in platinum replicas of freeze-dried cytoskeletons. *J. Cell Biol.* 86:212–234.

9. Heuser, J. E., T. S. Reese, M. J. Dennis, Y. Jan, L. Jan, and L. Evans. 1979. Synaptic vesicle exocytosis captured by quick freezing and correlated with quantal transmitter release. *J. Cell Biol.* 81:275–300.

10. Hodge, A. J., and W. J. Adelman, Jr. 1980. The neuroplasmic network in *loligo* and *hermissenda* neurons. *J. Ultrastruct. Res.* 70:220–241.

11. Ishikawa, H., R. Bischoff, H. Holtzer. 1969. Formation of arrowhead complexes with heavy meromyosin in a variety of cell types. *J. Cell Biol.* 43:312–328.

12. Ishikawa, H., S. Tsukita, and S. Tsukita. 1981. Ultrastructural aspects of the plasmalemmal undercoat. *In* Nerve Membrane. G. Matsumoto, and M. Kotani, editors. University of Tokyo Press, 167–183.

13. Jockusch, H., B. M. Jockusch, and M. M. Burger. 1979. Nerve fibers in culture and their interaction with non-neural cells visualized by immunofluorescence. *J. Cell Biol.* 80:629–641.

14. Kakiuchi, S., K. Sobue, K. Kanda, K. Morimoto, S. Tsukita, S. Tsukita, H. Ishikawa, and M. Kurokawa. 1982. Correlative biochemical and morphological studies of brain calspectin: a spectrin-like calmodulin-binding protein. *Biomed. Res.* 3:400–410.

15. Kobayashi, T., S. Tsukita, S. Tsukita, Y. Yamamoto, and G. Matsumoto. 1985. Subaxolemmal cytoskeleton in squid giant axon. I. Biochemical analysis of microtubules, microfilaments, and their associated high-molecular-weight proteins. *J. Cell Biol.* 102:1699–1709.

16. Kuczmarski, E. R., and J. L. Rosenbaum. 1979. Studies on the organization and localization of actin and myosin in neurons. *J. Cell Biol.* 80:356–371.

17. Lasek, R. J., and P. N. Hoffman. 1976. The neuronal cytoskeleton, axonal transport, and axonal growth. *In* Cell Motility. R. Goldman, T. Pollard, and J. Rosenbaum, editors. Cold Spring Harbor Laboratory, New York. 1021–1049.

18. Levine, J., and M. Willard. 1981. Fodrin: axonally-transported polypeptides associated with the internal periphery of many cells. *J. Cell Biol.* 90:631–643.

19. Matsumoto, G., M. Ichikawa, A. Tasaki, H. Murofushi, and H. Sakai. 1983. Axonal microtubules necessary for generation of sodium current in squid giant axons. I. Pharmacological study on sodium current and restoration of sodium current by microtubule proteins and 260 K protein. *J. Membr. Biol.* 77:77–91.

20. Matsumoto, G., T. Kobayashi, and H. Sakai. 1979. Restoration of the excitability of squid giant axon by tubulin–tyrosine ligase and microtubule proteins. *J. Biochem.* 86:155–158.

21. Metuzals, J., A. Hodge, R. J. Lasek, and I. R. Kaiserman-Abramof. 1983. Neurofilamentous network and filamentous matrix preserved and isolated by different techniques from squid giant axon. *Cell Tissue Res.* 228:415–432.

22. Metuzals, J., and I. Tasaki. 1978. Subaxolemmal filamentous network in the giant nerve fiber of the squid (*Loligo pealei L.*) and its possible role in excitability. *J. Cell Biol.* 78:597–621.

23. Morris, J. R., and R. J. Lasek. 1982. Stable polymers of the axonal cytoskeleton: the axoplasmic ghost. *J. Cell Biol.* 92:192–198.

24. Morris, J. R., and R. J. Lasek. 1984. Monomer-polymer equilibria in the axon: direct measurement of tubulin and actin as polymer and monomer in axoplasm. *J. Cell Biol.* 98:2064–2076.

25. Murofushi, H., Y. Minami, G. Matsumoto, and H. Sakai. 1983. Bundling of microtubules in vitro by a high molecular weight protein prepared from the squid axon. *J. Biochem.* 93:639–650.

26. Narahashi, T., N. C. Anderson, and J. W. Moore. 1967. Comparison of tetrodotoxin and procaine in internally perfused squid giant axons. *J. Gen. Physiol.* 50:1413–1428.

27. Peters, A. 1968. The morphology of axons of the central nervous system. *In* The Structure and Function of Nervous Tissue, Vol. 1. G. H. Bourne, editor. Academic Press, New York and London. 141–186.

28. Repasky, E. A., B. L. Granger, and E. Lazarides. 1982. Widespread occurrence of avian spectrin in nonerythroid cells. *Cell.* 29:821–833.

29. Sakai, H., and G. Matsumoto. 1978. Tubulin and other proteins from squid giant axon. *J. Biochem.* 83:1413–1422.

30. Sakai, H., G. Matsumoto, and H. Murofushi. 1985. Role of microtubules and axolinin in membrane excitation of the squid giant axon. *Adv. Biophys.* 19:43–89.

31. Shaw, G., M. Osborn, and K. Weber. 1981. Arrangement of neurofilaments, microtubules, and microfilament-associated proteins in cultured dorsal root ganglia cells. *Eur. J. Cell Biol.* 24:20–27.

32. Tsukita, S., and H. Ishikawa. 1981. The cytoskeleton in myelinated axons: serial section study. *Biomed. Res.* 2:424–437.

33. Tsukita, S., S. Tsukita, and H. Ishikawa. 1980. Cytoskeletal network underlying the human erythrocyte membrane. Thin-section electron microscopy. *J. Cell Biol.* 85:567–576.

34. Tsukita, S., S. Tsukita, H. Ishikawa, M. Kurokawa, M. Morimoto, K. Sobue, and S. Kakiuchi. 1983. Binding sites of calmodulin and actin on the brain spectrin, calspectin. *J. Cell Biol.* 97:574–578.

35. Tsukita, S., S. Tsukita, H. Ishikawa, S. Sato, and M. Nakao. 1981. Electron microscopic study of reassociation of spectrin and actin with the human erythrocyte membrane. *J. Cell Biol.* 90:70–77.

36. Tsukita, S., S. Tsukita, J. Usukura, and H. Ishikawa. 1983. ATP-dependent structural changes of the outer dynein arm in *Tetrahymena* cilia: a freeze-etch replica study. *J. Cell Biol.* 96:1480–1485.

37. Tsukita, S., J. Usukura, S. Tsukita, and H. Ishikawa. 1982. The cytoskeleton in myelinated axons: a freeze-etch replica study. *Neuroscience.* 7:2135–2147.

38. Tyler, J. M., and D. Branton. 1981. Rotary shadowing of extended molecules dried from glycerol. *J. Ultrastruct. Res.* 71:95–102.

39. Usukura, J., H. Akahori, H. Takahashi, and E. Yamada. 1983. An improved device for rapid freezing using liquid helium. *J. Electron Microsc.* 32:180–185.

40. Willard, M., M. Wiseman, J. Levine, and P. Skene. 1979. Axonal transport of actin in rabbit retinal ganglion cells. *J. Cell Biol.* 81:581–591.